ELSEVIER

Polymer 44 (2003) 681–689

polymer

www.elsevier.com/locate/polymer

Characteristics of polyvinylpyrrolidone-layered silicate nanocomposites prepared by attrition ball milling

Chong Min Koo, Hyeong Taek Ham, Min Ho Choi, Sang Ouk Kim, In Jae Chung*

Department of Chemical and Biomolecular Engineering, Korea Advanced Institute of Science and Technology, 373-1 Kusong-dong, Yusong-gu, Taejon 305-701, South Korea

Received 23 July 2002; received in revised form 25 October 2002; accepted 1 November 2002

Abstract

Polyvinylpyrrolidone (PVP)/sodium montmorillonite (MMT) nanocomposites prepared via the solution intercalation method were investigated by UV/vis, SEM, X-ray diffraction, TEM, FT-IR and PLM (polarized light microscopy). PVP/MMT nanocomposites show exfoliation below 20 wt% MMT and intercalation above this concentration. Nanocomposites retain good optical clarity and increased thermal resistance with MMT content. The compatibility between PVP and MMT and their enhanced properties may be explained by hydrogen bonding interactions. In addition, the nanocomposites prepared under more rigorous mixing conditions show better transparency because the smaller particle sizes are induced. In addition, the study on optically clear PVP/MMT suspensions helps one to understand how optical anisotropy of MMT is affected by the existence of polymer in aqueous solution.

Keywords: Polyvinylpyrrolidone nanocomposites; Hydrogen bonding; Optical anisotropy

1. Introduction

Polymer-layered silicate nanocomposites (PLSNs) have attracted a great attention, because they have shown dramatic improvements in mechanical, thermal and barrier properties with a small amount of layered silicates [1–9].

To understand the PLSNs, the microstructure of silicates must be considered. The *crystallite* (*tactoids*) consists of stacks containing between 10 and 100 parallel, equally spaced silicate platelets; each platelet is approximately 200 nm in length and 1 nm in thickness. The *primary particles* with a major dimension of several tens of microns, generally consist of a compact stack of individual silicate crystallite. From the microstructure point of view in the crystallite in PLSN, PLSN may have one of the following two morphologies. *Intercalated* structure has well ordered multi-layers in which the extended polymer chains are inserted. *Exfoliated* structure resulted from the separation of silicate layers, which keep the gap between layers wide enough for adjacent layers not to interact. The dispersion state of silicates in a polymer has tremendous effect on the properties of PLSNs. For example, an ideal exfoliated state is one of the ultimate aims in the fabrication of PLSN, because it has homogenously dispersed silicate plates in a polymer matrix.

PLSNs can be used as a model system not only for studying the polymer chain dynamics with the confined geometry [10–17], but also for the thermodynamic phase behavior of polymer–nanoparticle mixture [18–23]. Recently, Balazs and coworkers conducted a simulation based on the analytical self-consistent theory (SCF), where they considered both the concentration of silicate and the interactions among polymer, silicate and organic modifier. As a result, they showed that various mesophases should be formed in the nanocomposite with monodisperse silicate plates [19–23]. Koo and coworkers [18] reported that the highly filled maleated polyethylene-layered silicate nanocomposites could show the optical anisotropy from the ordering of layered silicates. However, we are not sure that the anisotropy is from intrinsic property of layered silicates in polymer or not, because the history of preparing the nanocomposites during melt blending may have extrinsic effect on the properties of nanocomposite.

PLSNs can be prepared from the various methods, such as solution intercalation [16,17,24–31], in situ polymerization [1–3,13–15], direct melt intercalation [4–12], and in situ synthesis of clay minerals in the presence of polymers

* Corresponding author. Tel.: +82-42-869-3916; fax: +82-42-869-3910.
E-mail address: chung@kaist.ac.kr (I.J. Chung).

0032-3861/03/$ - see front matter © 2002 Elsevier Science Ltd. All rights reserved.
PII: S0032-3861(02)00803-0

[32]. Among them, solution intercalation is one of the simplest methods if a polymer and layered silicates are dispersed in a solvent and the polymer is intercalated into the silicate layers during mixing the solution and removing the solvent. Furthermore, the nanocomposite prepared by the solution intercalation is a good model system for studying the phase behavior of PLSNs, because the historical effect during preparation is negligible over the whole range of silicate contents. Water-soluble polymers such as poly(vinyl-pyrrolidone) (PVP) [25–27,32], poly (vinyl alcohol) (PVA) [28,29] and poly(ethylene oxide) (PEO) [16,17,30] can easily intercalate into sodium montmorillonite (MMT) without hydrophobic treatments. Especially, PVP and its derivatives soluble in water as well as in many organic solvents, which have been used as a pigment dispersant, as a bonding agent, as a film-former, as a membrane, as a suspension stabilizer in medical fields, as a ink-receptor modifier, and so on, have been studied on fabrication of its nanocomposite [25–27,32]. However, a handful of intercalated nanocomposites have been reported.

In this work, PVP/MMT nanocomposites has been studied by changing the contents of MMT, which gives tremendous effect on the microstructure, their properties and anisotropic phase formation. Especially, this article shows why much more rigorous mixing during sample preparation is good for obtaining an optically transparent nanocomposites.

2. Experimental

2.1. Materials

The layered silicate was MMT from Kunimine Ind. Co. The cationic exchange capacity (CEC) of MMT was 119 meq/100 g. No particle size selection was carried out. PVP ($M_w = 55\,000$) was purchased from Aldrich. Deionized water (H_2O) was used as solvent at room temperature.

2.2. Preparation of PVP/MMT nanocomposites

PVP/MMT nanocomposite was prepared by two methods to investigate the effect of mixing condition on the properties. One is simple stirring. The other is more rigorous mixing by using attrition ball milling, in which zirconium balls with diameter of 1 mm was used at 300 rpm in the zirconium jar. MMT was dispersed for 2 weeks in water for sufficient wetting before adding PVP. The concentration of solute was kept below 7 wt%. PVP/MMT/H_2O suspensions were prepared by stirring for 1 week after adding PVP. Nanocomposite films were obtained by casting the PVP/MMT/H_2O suspensions.

2.3. Characterization of PVP/MMT nanocomposites

The turbidity was measured by using a digital camera. Transparency of the cast film was measured by using UV/vis spectrophotometer (Duksan Mecasys Optizen II). The surface morphologies of the cast film were observed by scanning electron microscopy (SEM, LEO 1455VP). The periodic structure and the orientation of PVP/MMT nanocomposite films were evaluated by wide angle X-ray diffraction (WAXD) (Rigaku X-ray generator, Cu Kα radiation, $\lambda = 0.15406$ nm) and D8 Discover X-ray diffractometer (Bruker), respectively. The morphology of the thin film of nanocomposite prepared by ultra-microtome (RMC, MT-XL) was observed by transmission electron microscope (TEM, Philips CM-20). Thin film was cut perpendicular to the surface direction and laid on the copper grid in dry state because PVP is a water-soluble polymer. The accelerating voltage of TEM was 120 kV. Infrared spectra for the cast film on Si wafer, were recorded on a Bomem 102 FT-IR spectrometer with resolution of 2 cm^{-1}. Thermogravimetric analysis (TGA) was performed on a thermogravimetric analyzer (TA instruments) with a Perkin–Elmer thermobalance at heating rate of 10 °C/min under nitrogen atmosphere.

2.4. Characterization of PVP/MMT/H_2O suspensions

The colorless transparent PVP/MMT suspensions prepared by attrition ball milling were used to investigate optical anisotropy. The birefringence of samples was studied between two crossed polarizers, using test tubes of 13 mm diameter, and by a polarized light microscopy (PLM, A Leitz, Model Laborlux 12 Pols).

3. Results and discussion

3.1. The effect of mixing condition in the preparation of PVP/MMT nanocomposites

Fig. 1 shows the photographs of PVP/MMT suspensions prepared by two different mixing methods (i.e. simple

Fig. 1. Photographs for PVP/MMT suspensions. (a) StP0M100 suspensions of MMT concentration of 0.015 g/ml. (b) AtP0M100 suspensions of MMT concentration of 0.015 g/ml. (c) StP80M20 suspension of MMT concentration of 0.022 g/ml and (d) AtP80M20 suspension of MMT concentration of 0.022 g/ml.

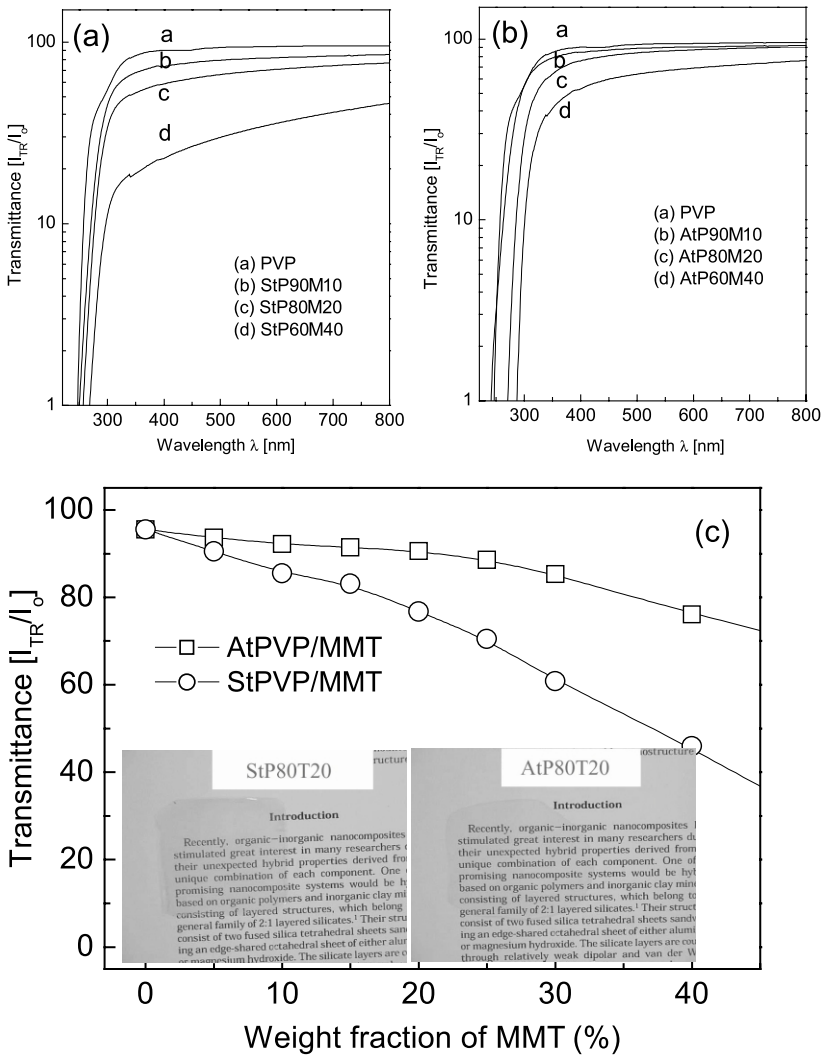

Fig. 2. UV/vis spectra of (a) StPVP/MMT and (b) AtPVP/MMT cast films. (c) Transmittance of the nanocomposite films at 700 nm of visible region. Insets show photographs of StP80M20 and AtP80M20 films with the thickness of about 100 μm.

stirring and more rigorous stirring by attrition ball milling). No particle size selection of MMT was carried out. Test tubes with diameter of 13 mm containing typically 3 ml of suspensions were used. In the name of samples, the letters St, At, P and M denote simple stirring, attrition ball milling, PVP and MMT, respectively. The numbers followed after P and M stand for weight percents of materials based on amount of total solutes (PVP and MMT). The concentration of MMT in aqueous solution ranges from 0.015 to 0.022 g/ml. The PVP/MMT/H_2O suspensions look different according to their preparation methods. The simply stirred suspensions of Fig. 1(a) and (c) are very opaque at each concentration. The opaqueness does not improve after further stirring. The prolonged dispersion stability is also not good. On the other hand, the attrition ball-milled suspensions of Fig. 1(b) and (d) are visually non-scattering and look slight yellowish. No precipitation is observed upon prolonged standing over 6 months. This result indicates that the simply stirred suspensions is big enough to be responsible for visual scattering, on the other hand, attrition ball-milled suspensions is too small to appear visual scattering.

Fig. 2 shows UV/vis transmittance spectra of StPVP/MMT and AtPVP/MMT nanocomposite films with thickness of about 100 μm and the comparison of transmittances of both nanocomposite series at 700 nm of visible region. All samples show higher absorption in the UV light than in the visible light (400–800 nm). The transmittance of both nanocomposite films monotonically reduces with the concentration of silicates. Insets in Fig. 2(c) show photographs of StP80M20 and AtP80M20 films with the thickness of about 100 μm. Both films even with 20 wt% MMT contents keep the good optical clarity. AtP80M20 film shows much higher transparency than StP80M20 film. AtPVP/MMT nanocomposites have the higher transmittance than StPVP/MMT regardless of MMT contents.

Fig. 3 shows X-ray diffraction patterns of StPVP/MMT and AtPVP/MMT nanocomposite films. The peaks in X-ray

Table 1
Characterization of StPVP/MMT and AtPVP/MMT nanocomposites

MMT content (wt%)	2θ (degree) (d-spacing (nm))									
	5	10	15	20	25	30	40	60	80	100
StPVP/MMT	–	–	–	1.58 (5.58)	1.77 (4.96)	1.82 (4.85)	2.27 (3.89)	3.08 (2.87)	4.39 (2.01)	7.19 (1.23)
AtPVP/MMT	–	–	–	1.56 (5.66)	1.72 (5.13)	2.12 (4.16)	2.27 (3.89)	3.07 (2.87)	4.38 (2.02)	7.19 (1.23)

diffraction patterns correspond to (001) plane reflection peaks of layered silicates. The *d*-spacings calculated by Bragg's law are listed in Table 1. The *d*-spacing of MMT is about 1.26 nm. X-ray diffraction patterns of StPVP/MMT change much with the concentration of silicates. The (001) reflection peak does not appear up to the silicate concentration of 15 wt% but appears above 20 wt%. It indicates that the StPVP/MMT nanocomposites have the exfoliated morphology up to 15 wt% silicate contents and the intercalated morphology above 20 wt%. The *d*-spacing between adjacent silicate layers gradually decreases with the concentration of silicates in intercalation region. The existence of exfoliation at the low concentration means that PVP has the good compatibility with MMT. Despite the significant difference of transparency between StPVP/MMT and AtPVP/MMT in aqueous solution and cast-films, however,

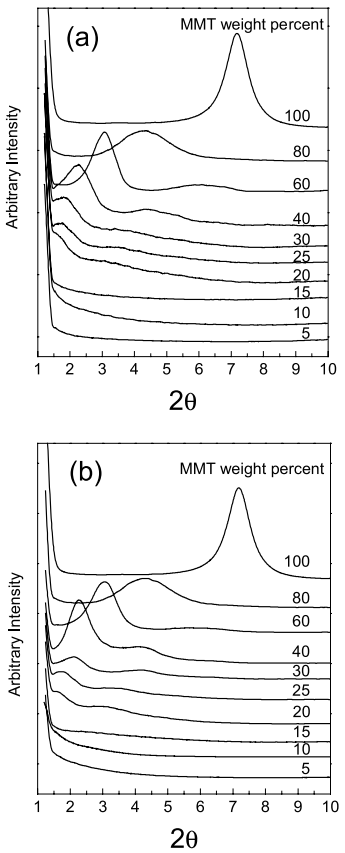

Fig. 3. X-ray diffraction patterns of (a) StPVP/MMT and (b) AtPVP/MMT cast films.

AtPVP/MMT nanocomposite show almost the same X-ray diffraction patterns as StPVP/MMT.

Fig. 4 shows SEM photographs of StP0M100, AtP0M100, StP75M25 and AtP75M25 thin films. All films are cast on the silicone wafer. In StP0M100, one can see the very rough surface with a lot of big aggregated particles with major axis dimension of a few tens of microns. On the other hand, AtP0M100 has the very smooth surface. The aggregated particles are not observed in AtP0M100 even at micron scale. In the case of StP80M20 and AtP80M20, it is not easy to observe the particles due to PVP matrix polymer, which covers the surface. However, it is clear that AtP80M20 has much smoother surface than StP80M20. It could be concluded from Fig. 4 that the particle size in the nanocomposite became much smaller after more rigorous attrition ball milling. It must be the reason why AtPVP/MMT shows higher transparency than StPVP/MMT in Figs. 1 and 2.

3.2. The microstructure and characterization of PVP/MMT nanocomposites

Fig. 5 shows X-ray photographs for AtP100M0, AtP90M10, AtP60M40 and AtP20M80 nanocomposite films. X-ray beam was incident on an as-cast film in the through and edge directions. Edge and through directions were perpendicular and parallel to surface normal direction of the film, respectively. For the edge-view experiment, a line of edge of nanocomposite film was laid in the direction shown by arrow in Fig. 5(a). Pure PVP shows the very weak isotropic intensity distribution in both edge-view and through-view photographs. It indicates PVP has the very low crystallinity and its crystals are distributed randomly. On the other hand, the photographs of nanocomposites highly depend on the direction of incident X-ray beam. The characteristic reflection originating from the periodicity of silicate layers near the beam stopper is shown in the edge-view photographs, not in the through-view photographs. Especially, in the edge-view photographs, it is found that the reflections of nanocomposites near the beam stopper being inclined at $+45°$ in the images represents that the silicate surfaces are aligned parallel to the film surface. On casting the nanocomposite suspensions on the Si wafer, the silicate platelets with large aspect ratio in the suspensions prefer to orient parallel to film surface because it is the most stable state. The well-aligned silicate structure might be expected

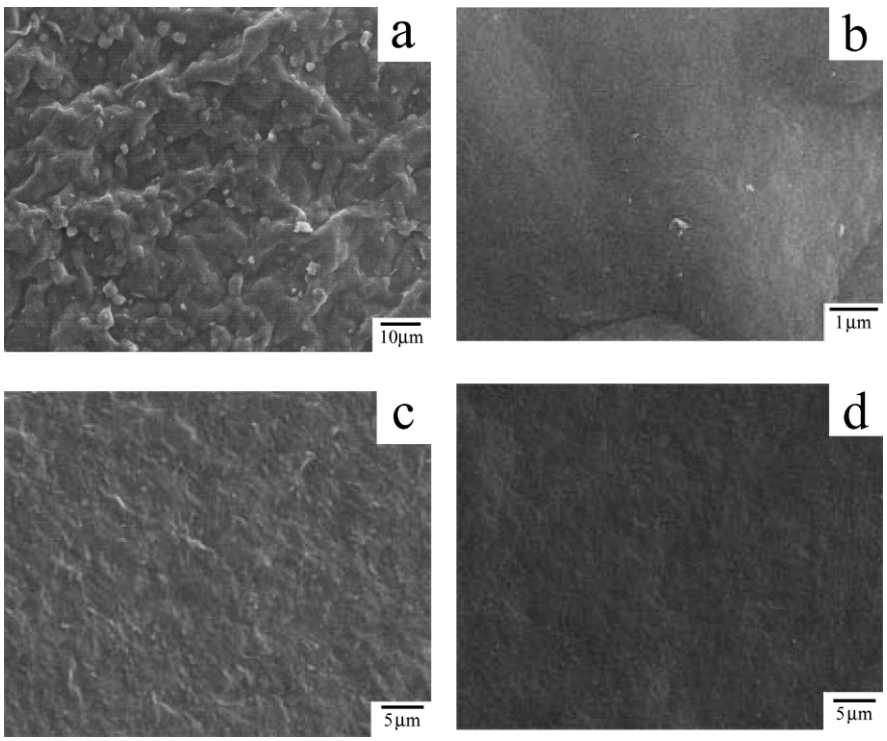

Fig. 4. Scanning electron micrographs of (a) StP0M100, (b) AtP0M100, (c) StP80M20 and (d) AtP80M20 films cast on the silicone wafer.

the enhanced barrier properties. In addition, AtP90M10 has a reflection around the beam stopper. It is a typical 2-D SAXS pattern of exfoliated nanocomposite [18,24,29]. AtP80M40 and AtP20M80 have a pair of reflections near the beam stopper. The additional outer reflection corresponding to (001) reflection is observed in the intercalation, not in the exfoliation [18,24,29]. It agrees well with Fig. 3.

Fig. 6 shows transmission electron micrographs of AtP90M10 and AtP80M20 nanocomposite films. The line of edge in the nanocomposite film corresponds to vertical direction in the images. Dark lines in the images represent the silicate layers. Silicate layers have mean length of about 150 nm and uniform thickness of about 1 nm. In Fig. 6(a), one can observe that individual silicate layers are well dispersed in the nanocomposites. It is hard to observe clay aggregates in the whole area. AtP90M10 nanocomposite has the exfoliated morphology, which agrees well with the result of Fig. 3. On the other hand, AtP80M20 nanocomposite shows quite different image. The silicate layers show the tightly stacked layer structure, the intercalated morphology. Mean layer spacing is consistent with the layer spacing of 5.6 nm in Fig. 3. In addition, it is observed that surface direction of silicate platelets in both photographs highly orient parallel to surface direction of film as expected. From the observations of X-ray diffraction and TEM, we can conclude that PVP and MMT are considerably compatible enough to form an exfoliated nanocomposite up to 15 wt% MMT contents. Above 20 wt%, they may form an intercalated nanocomposite. The morphology evolution with MMT appears because interaction between adjacent silicate layers becomes stronger than favorable interaction between PVP and silicates as average distance between silicate layers decreases with the concentration of MMT content [18].

Fig. 7 shows TGA thermograms of weight loss as a function of temperature for AtPVP/MMT nanocomposites. The thermal decomposition temperature increases a little and weight loss decreases as the silicate content increases. It indicates the thermal stability of PVP improves with MMT.

Fig. 8(a) shows the infrared spectra of PVP, AtPVP/MMT nanocomposites, and MMT. In spectrum of PVP, CH stretching 2937 cm^{-1}, C=O stretching 1650 cm^{-1}, CH_3 scissoring 1420 − 1500 cm^{-1}, C–C ring stretching 1370 cm^{-1} and tertiary amine C–N stretching 1290 cm^{-1} reveal the characteristic absorbance bands of PVP [25]. In spectrum of MMT, Si–O stretching 1026 cm^{-1} and OH stretching 3630 cm^{-1} reveal [3,5]. AtPVP/MMT nanocomposites show the characteristic absorbance bands of both PVP and MMT at the same peak positions. Unexpectedly, C=O peak position shows an apparent downward shift from 1670 to 1650 cm^{-1} with the concentration of silicates as magnified in the insect. Such down shift may be due to three reasons; hydrogen bonding (H-bonding) interaction between C=O of PVP and hydroxyl group (OH) of water, an interaction between C=O and sodium cation from MMT, and H-bonding interaction between C=O and OH on the silicate surface [25]. First, in Fig. 8(a), all specimens contain a little water at almost the same level, which is confirmed from strong and broad peak around 3500 cm^{-1}. Thus, H-bonding between carbonyl and water can be negligible. Second, Fig. 8(b) shows the infrared spectra of PVP films

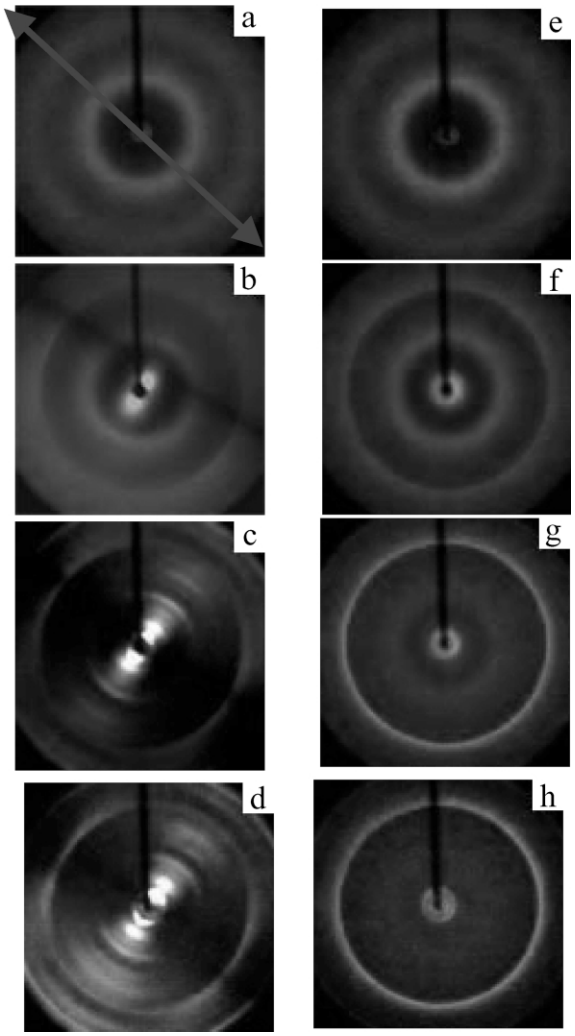

Fig. 5. X-ray diffraction photographs of AtPVP/MMT nanocomposite films containing the MMT content of (a) 0, (b) 10, (c) 40 and (d) 80 wt% in the edge-view experiments and (e) 0, (f) 10, (g) 40 and (h) 80 wt% in the through-view experiments.

with or without sodium chloride to examine the effect of sodium cation. The peak position of C=O is not affected by addition of sodium cation. Therefore, down shift of carbonyl group band of PVP must be caused by the formation of H-bonding interaction between C=O of PVP and OH on the silicate surface. The H-bonding interaction may enhance the compatibility between PVP and MMT. That might be why PVP exfoliates into MMT up to 15 wt% MMT concentration as well as PVP/MMT nanocomposite shows the enhanced thermal property.

3.3. Anisotropy formation of PVP/MMT nanocomposites

Non-spherical all-inorganic or mineral particles, such as V_2O_5, imogolite, boehmite, gibbsite, nickel (II) hydroxide and clay in solvent or water, can form liquid crystalline mesophase [33–39]. Particularly, smectite clays in water, where an electrostatic interaction between silicate platelets

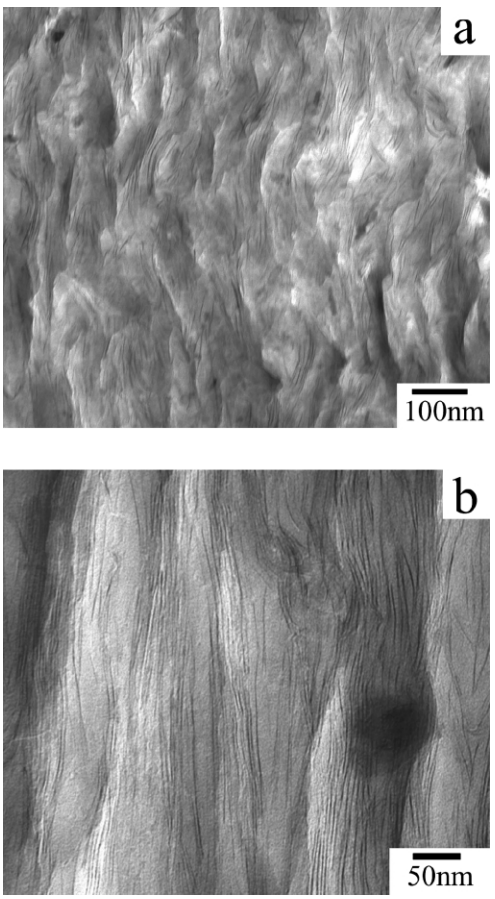

Fig. 6. Transmission electron micrographs of (a) AtP90M10 and (b) AtP80M20.

helps the formation of anisotropic phase, starts to form the nematic phase above about 2 wt% clay concentration in aqueous solution [36–39]. In recent, Koo and coworkers [18] reported that the highly filled maleated polyethylene-layered silicate nanocomposites with a negligible electrostatic

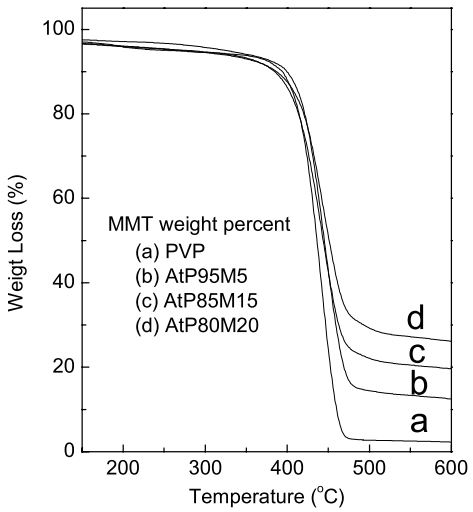

Fig. 7. TGA thermograms of weight loss as a function of temperature for (a) PVP, (b) AtP95M5, (c) AtP85M15 and (d) AtP80M20. The numbers in the insets show the weight percents of MMT in the suspensions.

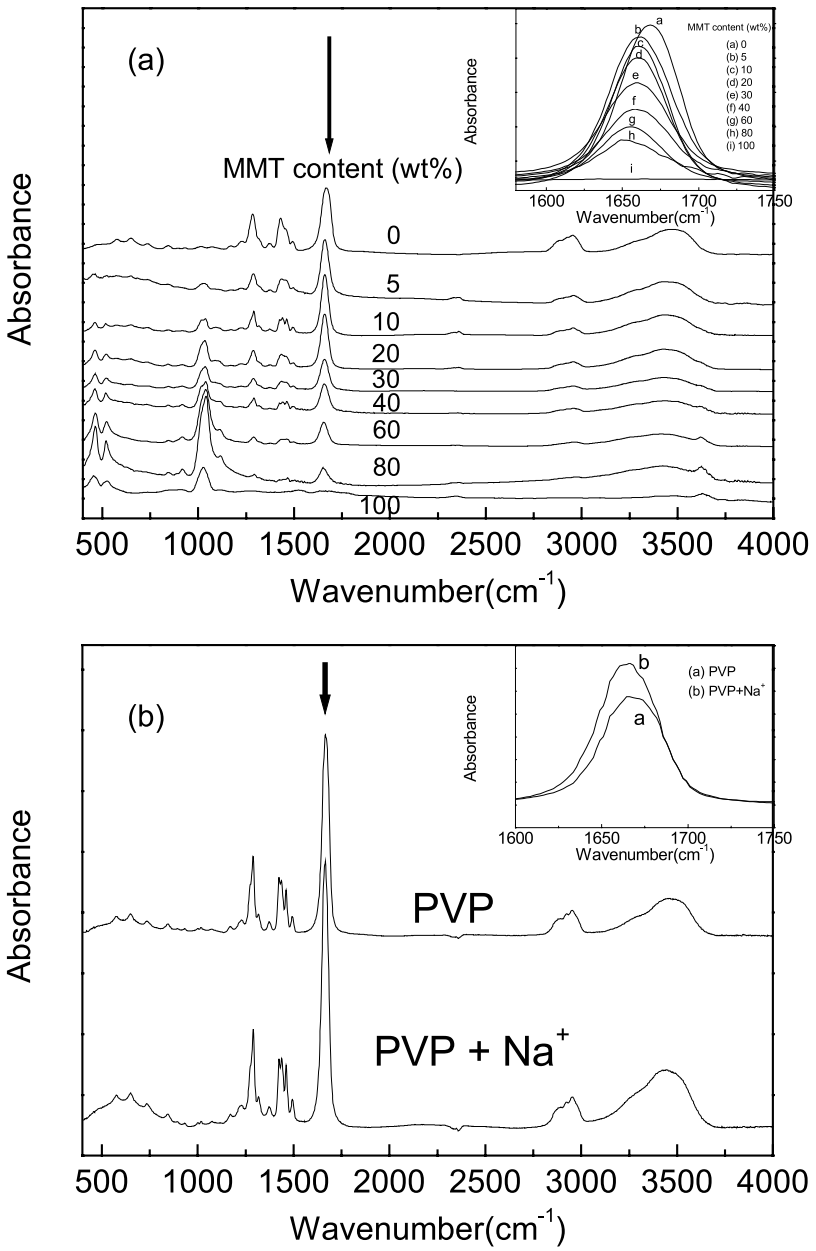

Fig. 8. (a) FT-IR spectra of AtPVP/MMT nanocomposite films and (b) FT-IR spectra of PVP films with or without sodium. Details of the carbonyl band is given in the inset.

interaction form the optical anisotropy above 12 vol% (≈20 wt%) of organically modified silicates. The transparent AtPVP/MMT suspensions can be used as a model system for studying how polymer affects the anisotropic phase formation of silicate layers in the polymer/MMT aqueous solution.

Fig. 9 shows the photographs of AtP0M100 suspensions with various concentrations. The tubes filled with suspensions between crossed polarizers, look different according to their concentrations. The suspensions having lower than a threshold concentration of MMT, $C_{MMT} = 0.025 \pm 0.002$ g/ml for AtP0M100, look dark at macroscale. Darkness indicates the optically isotropic state. In contrast, the suspensions above the threshold concentration appear birefringent. The optical anisotropy gets stronger with the

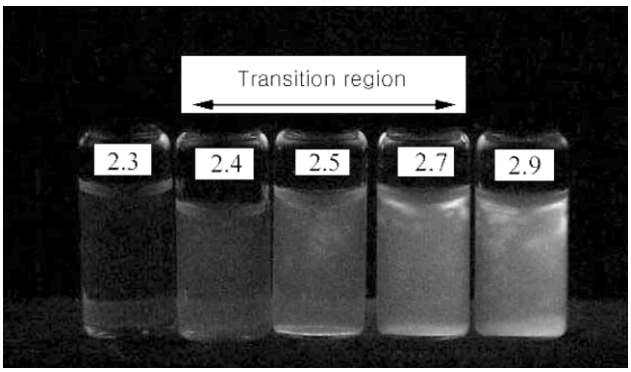

Fig. 9. Photographs of AtP0M100 suspensions at various MMT concentrations between crossed polarizers.

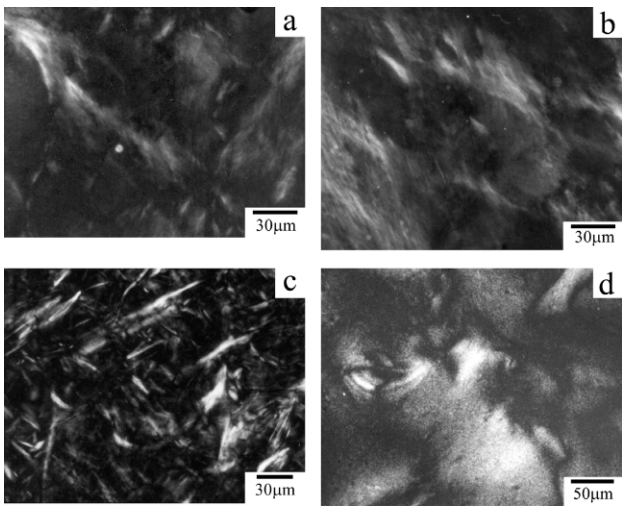

Fig. 10. Polarized light micrographs of (a) AtP90M10, (b) AtP80M20, (c) AtP10M80 and (d) AtP0M100 suspensions above the threshold concentrations.

concentration of MMT. However, the suspensions do not exhibit a clear onset point of biphasic region as reported [36–39], because the transition concentration at which birefringence starts, is larger than the gelation concentration in the case of clay suspensions [39]. From time to time, the transition concentration is difficult to be observed for gel sample because they take a long time to reach equilibrium. Despite of this problem, the isotropic to anisotropic transition concentration can be determined within ±0.002 g/ml accuracy as shown in Fig. 9.

Fig. 10 shows polarized light micrographs of AtPVP/MMT suspensions with different PVP/MMT ratios above threshold values. All photographs show the clear optical anisotropy. It is clear that the anisotropy must be originated from ordering of the hard clay platelets because PVP is a typical flexible polymer.

Fig. 11 shows the phase diagram specifying the transition from isotropic to anisotropic phase of AtPVP/MMT suspensions. C_{total} and C_{MMT} indicate total solute (PVP and MMT) concentration and MMT concentration in the suspensions at the isotropic to anisotropic phase transition, respectively. The abscissa represents the weight fraction of MMT based on total solutes. C_{total} decreases sharply with the increase of relative MMT concentration. C_{MMT} for single MMT suspensions, AtP0M100 is 0.025 ± 0.002 g/ml. C_{MMT} decreases gradually with the decrease of relative MMT concentration and decreases sharply below 20 wt% MMT contents. It means that the existence of PVP in suspensions helps silicate platelets form optical anisotropy at the lower concentration.

4. Conclusion

Water-soluble PVP/MMT nanocomposites prepared via solution intercalation method were investigated by using UV/vis, SEM, X-ray diffraction, TEM and PLM. The

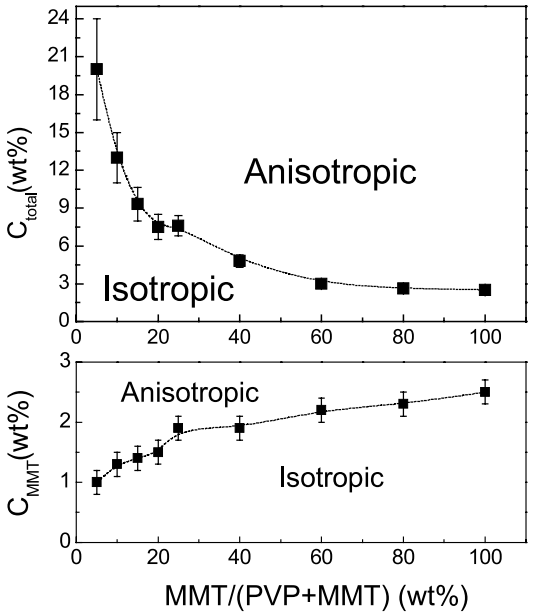

Fig. 11. The phase diagram specifying the transition from isotropic to anisotropic phase of AtPVP/MMT suspensions.

nanocomposites prepared by attrition ball milling show better optical transparency than the ones by simple stirring because the more rigorous mixing can induce the smaller sizes of tactoid or primary particle in the nanocomposites. PVP and MMT are considerably compatible enough to form an exfoliated nanocomposite up to 20 wt% MMT contents. Above the 20 wt%, they may form an intercalated nanocomposite. PVP/MMT nanocomposites keep the good optical transparency and show the enhanced thermal resistance with MMT loading. These results could be assisted by the hydrogen bonding interaction between C=O of PVP and OH on the silicate surface. In the investigation of optical anisotropy for the optically clear AtPVP/MMT suspensions, the isotropic to anisotropic phase transition concentration of MMT decreases with the increase of relative PVP concentration.

Acknowledgements

This work was supported in part by Brain Korea 21 program and in part by the Center for Advanced Functional Polymers. We thank Samsung General Chemicals for allowing the use of the cryogenic ultra-microtome.

References

[1] Kojima Y, Usuki A, Kawasumi M, Okada A, Fukushima Y, Kurauchi T, Kamigaito O. J Mater Res 1993;8:1185.
[2] Kojima Y, Usuki A, Kawasumi M, Okada A, Kurauchi T, Kamigaito O. J Appl Polym Sci 1993;8:1185.
[3] Choi YS, Choi MH, Wang KH, Kim SO, Kim YK, Chung IJ. Macromolecules 2001;34:8978.

[4] Vaia RA, Vasudevan S, Krawiec W, Scanlon SG, Giannelis EP. Adv Mater 1995;7:154.
[5] Choi MH, Chung IJ, Lee JD. Chem Mater 2000;11:2977.
[6] Byun HY, Choi MH, Chung IJ. Chem Mater 2001;13:4221.
[7] Wang KH, Xu M, Choi YS, Chung IJ. Polym Bull 2001;46:499.
[8] Wang KH, Choi MH, Koo CM, Chung IJ. Polymer 2001;42:9819.
[9] Koo CM, Kim MJ, Choi MH, Kim SO, Chung IJ. HWAHAK KONGHAK 2001;39:635.
[10] Lim YT, Park OO. Rheol Acta 2001;40:220.
[11] Lim YT, Park OO. Macromol Rapid Commun 2000;21:231.
[12] Hoffmann B, Dietrich C, Thomann R, Friedrich C, Mulhaupt R. Macromol Rapid Commun 2000;21:57.
[13] Vaia RA, Jandt KD, Kramer EJ, Giannelis EP. Macromolecules 1995; 28:8080.
[14] Krishnamoorti R, Vaia RA, Giannelis EP. Chem Mater 1996;8:1728.
[15] Krishnamoorti R, Vaia RA, Giannelis EP. Macromolecules 1997;30: 4097.
[16] Hackett E, Manias E, Giannelis EP. Chem Mater 2000;12:2161.
[17] Bujdak J, Hackett E, Giannelis EP. Chem Mater 2000;12:2168.
[18] Koo CM, Ham HT, Kim SO, Wang KH, Chung IJ, Kim DC, Zin WC. Macromolecules 2002;35:5116.
[19] Lyatskaya Y, Balazs AC. Macromolecules 1998;31:6676.
[20] Balazs AC, Singh C, Zhulina E, Lyatskaya Y. Acc Chem Res 1999; 32:651.
[21] Ginzburg VV, Balazs AC. Macromolecules 1999;32:5681.
[22] Ginzburg VV, Singh C, Balazs AC. Macromolecules 2000;33:1089.
[23] Ginzburg VV, Balazs AC. Adv Mater 2000;12:1805.
[24] Jimenez G, Ogata N, Kawai H, Ogihara T. J Appl Polym Sci 1997;64: 2111.
[25] Francis CW. Soil Sci 1973;115:40.
[26] Levy R, Francis CW. J Colloid Interf Sci 1975;50:442.
[27] AdsoGultex A, Seckin T, Yunusona L, Icduygu MG. J Appl Polym Sci 2001;81:512.
[28] Strawhecker KE, Manias E. Chem Mater 2000;12:2943.
[29] Ogata N, Kawakage S, Ogihara T. J Appl Polym Sci 1997;66:573.
[30] Vaia RA, Vasudevan S, Krawiec W, Scanlon LG, Giannelis EP. Adv Mater 1995;7:154.
[31] Fournaris KG, Karakassides MA, Petridis D. Chem Mater 1999;11: 2372.
[32] Carrado KA, Xu L. Chem Mater 1998;10:1440.
[33] Onsager L. Ann NY Acad Sci 1949;51:627.
[34] van der Kooij FW, Kassapidou K, Lekkerkerker HNW. Nature 2000; 406:868.
[35] Lekkerkerker HNW, Stroobants A. Nature 1998;393:305.
[36] Langmuir I. J Chem Phys 1938;6:873.
[37] Davidson P, Batail P, Gabriel JCP, Livage J, Sanchez C, Bourgaux C. Prog Polym Sci 1997;22:913.
[38] Gabriel JCP, Davidson P. Adv Mater 2000;12:9.
[39] Gabriel JCP, Sanchez C, Davidson P. J Phys Chem 1996;100:11139.